Chapter 8
Maximum Power Point Tracking (MPPT) Algorithms for Photovoltaic Systems

Ersan Kabalci

Abstract The solar energy have become a challenging area among other renewable energy sources (RESs) since the photovoltaic (PV) systems have the advantages of not causing pollution, having low maintenance, and long-lasting operation life. Besides these advantages, a PV system has several drawbacks such as considerably higher installation cost comparing some other RESs, and limited efficiency ranges between 9–18%. The feasibility analyses have a great role in order to determine the most appropriate plant site before installation. On the other hand, the operating analyses and improvements based on maximum power point tracking (MPPT) are quite important to increase the harvested total energy. The intermittent characteristic and perturbing power curve of a PV module is one of the most important defects that should be tackled to increase the generation efficiency. The power-voltage (P-V) and current-voltage (I-V) curves are main efficiency indicators of a PV system that exhibit nonlinear characteristics in its natural structure. Furthermore, the generated maximum power with a PV panel depends on two main quantities of temperature and irradiation. However, it is possible to increase the generated power up to maximum rates by MPPT algorithms. This chapter introduces most widely used algorithms respecting to their implementation and utilization properties. The indirect, direct, and computational methods are presented considering their advantages and disadvantages. The conventional and novel algorithms are explained with flowcharts and analytical details in order to provide clear comparison. The artificial methods are expressed in the last section where fuzzy logic, artificial intelligence, and optimization-based approaches are discussed.

Keywords Maximum power point tracking (MPPT) · Perturb and observe · Incremental conductance · Fuzzy logic controller · Artificial neural network · Particle swarm optimization

E. Kabalci (✉)
Faculty of Engineering and Architecture, Department of Electrical and Electronics Engineering, Nevsehir HBV University, Nevsehir, Turkey
e-mail: kabalci@nevsehir.edu.tr

N. Bizon et al. (eds.), *Energy Harvesting and Energy Efficiency*,
Lecture Notes in Energy 37, DOI 10.1007/978-3-319-49875-1_8

Abbreviation and Acronyms

ABC	Artificial Bee Colony
AF	Activation Function
ANN	Artificial Neural Network
COA	Centroid of Area
CV	Constant Voltage
EMI	Electromagnetic Interference
ESS	Energy Storage System
FLC	Fuzzy Logic Controller
GA	Genetic Algorithm
HC	Hill Climbing
IncCond	Incremental Conductance
I-V	Current-Voltage
MLI	Multilevel Inverter
MLP	Multilayer Perceptron
MPPT	Maximum Power Point Tracking
OV	Open Voltage
P&O	Perturb and Observe
PSO	Particle Swarm Optimization
PV	Photovoltaic
P-V	Power-Voltage
RES	Renewable Energy Source
SCPB	Short-Current Pulse-Based
THD	Total Harmonic Distortion

8.1 Chapter Overview

The maximum power point tracking (MPPT) is an algorithm that is associated with dc-dc power converters and inverters to track maximum power point during energy conversion process. Thus, the generated energy is maximized in this way. Although there are several methods proposed to implement an MPPT system, there are two algorithms known as "perturb and observe" (P&O) and the "incremental conductance" (IncCond methods are widely used since they are commercially preferred. However, simpler algorithms lack to provide the anticipated performance on the output power. The recent researches on MPPT algorithms exhibited that more sophisticated algorithms yield better outputs comparing to widely known basic methods. Therefore, a wide variety of numerical methods including fuzzy logic, neural networks and other computational methods are proposed. Although these recent algorithms require increased complexity, they easily compete with malfunctions of previous methods in terms of partial shading, misdirection during tracking, power fluctuations around MPP, and inadequate performance at low irradiance.

In this chapter, the MPPT algorithms have been analyzed in there groups where the first group includes indirect algorithms while others are described as direct algorithms, and numerical algorithms. The groups have been allocated considering the progress on methods and approaches where the indirect and direct algorithms are known as conventional MPPT techniques. The most recent computational algorithms including genetic algorithms, particle swarm optimization (PSO) algorithms, and artificial bee colony algorithms (ABC) are the hottest topics in MPPT algorithms. The trade-off between conventional MPPT methods and recent algorithms are related to complexity in algorithm and to cost in application.

This chapter is dedicated to these widely used MPPT algorithms of PV systems. Therefore, the initial sections introduce analytical background of a PV panel at a glance, and power curves of any PV panel in brief. Afterwards, the power conversion system of a PV plant with power converters is described to emphasize the application of a generic MPPT block in power conversion issues in the following section. The MPPT algorithms have been presented in three sections including indirect algorithms, direct algorithms, and numerical algorithms with their application examples.

8.2 Basic Principles of Photovoltaic Energy Conversion

Edmund Becquerel, a French physicist, firstly discovered the photovoltaic (PV) energy by generating electricity when he illuminated an electrode in electrolyte solution in 1839. However, Adams and Day made the first practical application of PV by applying the PV energy to solid materials about 40 years later. The primary PV cells made of selenium were performing almost 1 or 2% efficiency. Probably Einstein was the most important contributor of PV by explaining theoretical PV effect in 1904 that brought a Nobel Prize to him in 1923. The first generation silicon PV cells were produced by 1940s and 1950s by Czochralski, a Polish scientist. The solar panels constituted with numerous PV cells were commercially available in 1963 when Sharp Corporation succeeded in producing practical silicon photovoltaic modules. Although there were several applications of solar cells seen in Vanguard I space satellite in 1958, Explorer III, Vanguard II, and Sputnik-3 in 1959. World's first largest PV array was built in Japan with 242 Wp rated power in 1963 [1–4].

A PV energy conversion system is composed of a PV module, a dc-dc converter, an inverter, and preferably an energy storage system (ESS). The PV module is constituted by PV cells that are series and parallel connected to generate the desired rated power. The cells are produced in monocrystalline or polycrystalline structure depending to the purity of semiconductor [5–7]. The polycrystalline cells that provide limited efficiency around 13–14% are less efficient comparing to the monocrystalline that the efficiency increases up to 20%.

The analytical model of a PV cell is designed referring to one-diode electrical equivalent as shown in Fig. 8.1. This circuit includes a photocurrent source, a diode, and serial and shunt resistors that are known as *one-diode* or *five-parameter* model [8]. The calculations of the one-diode model seen in Fig. 8.1 are depended to the output current;

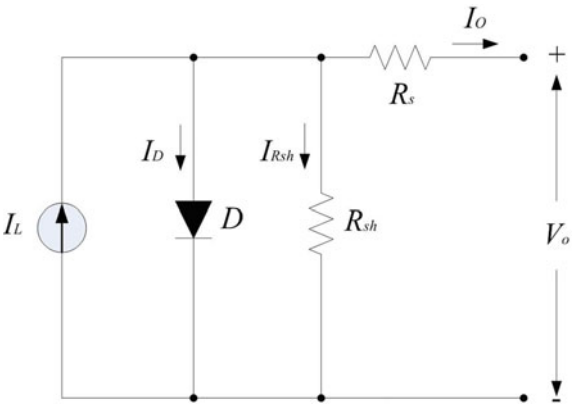

Fig. 8.1 Single-diode electrical equivalent of a mono or polycrystalline PV cell

$$I_o = I_{PV} - I_D(V) - I_{sh}(V) \tag{8.1}$$

where (V) depicts the dependency of diode and resistor currents to terminal voltage while they are independent from irradiation value.

The Shockley equation is called to express the semiconductor diode behavior to define I_D as given in Eq. (8.2);

$$I_D = I_R(e^{\frac{V_D}{\eta V_T}} - 1) \tag{8.2}$$

where I_D is current and V_D is voltage of the diode, I_R is reverse blocking current, V_D is thermal voltage, and η is the ideality factor of the diode [9, 10]. The current of shunt resistor I_{sh} is rearranged regarding to its dependence to terminal voltage as seen in (8.3);

$$I_{sh} = \frac{V_O + I_O R_S}{R_{sh}} \tag{8.3}$$

where the equivalence shown in Eq. (8.1) is achieved as seen in Eq. (8.4) referring to irradiation current I_{PV}, thermal voltage V_T, and other parameters denoted above [8–10];

$$I_O = I_{PV} - I_R\left(e^{\frac{V_O + I_O R_S}{\eta_I V_T}} - 1\right) - \frac{V_O + I_O R_S}{R_{sh}} \tag{8.4}$$

There are several other equivalent circuit models presented in the literature to increase the reliability of the PV cell design. The implementation structure of the cell is expressed by additional electrical elements in the improved models. One of these models that is being extensively studied one, amorphous silicon PV cell is illustrated in Fig. 8.2. The polymer and amorphous silicon based PV cell is constituted with an additional dependent current source controlled by photocurrent and terminal voltage.

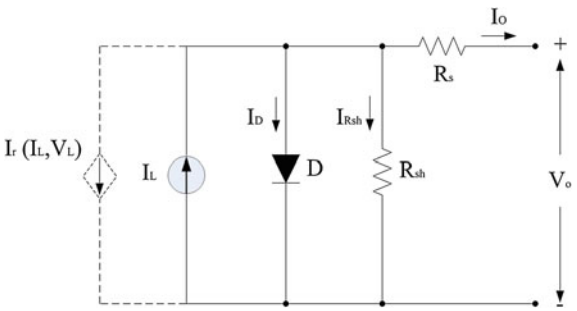

Fig. 8.2 Single-diode electrical equivalent of an amorphous silicon PV cell

This equivalent circuit is obtained by modifying the well-known five-parameter model, and the calculations are rearranged considering the dependent current source. The output current equation is rearranged by taking into account the additional dependent current source as seen in Eq. (8.5);

$$I_O = I_{PV} - I_D(V) - I_{sh}(V) - I_r(I_{PV}, V_L) \tag{8.5}$$

The photocurrent I_{PV} is proportional to the irradiation ψ where the dependent source current can be converted to $I_r(I_{PV}, V_L) = I_r(\psi, V_L)$. Since the output current of amorphous silicon PV cell is calculated regarding to the Eq. (8.6) that depicts the dependency of diode and shunt current to the irradiation and terminal voltage;

$$I_O = I_{PV} - I_D(\psi, V) - I_{sh}(\psi, V) \tag{8.6}$$

A PV module is composed of a number of series cells N_S as 36, 60, or 72 while the cells are connected in series and parallel N_P in PV arrays as shown in Fig. 8.3 where the arrangement defines the maximum output voltage V_M and maximum output current I_M. The maximum output currents of a module I_M and an array I_A are calculated regarding to Eq. (8.4) as follows [10–12];

$$I_M = I_{PV} - I_O\left(e^{\frac{V_M + I_M N_S R_S}{\eta_I N_S V_T}} - 1\right) - \frac{V_M + I_M N_S R_S}{N_S R_{sh}} \tag{8.7}$$

$$I_A = N_P I_{PV} - N_P I_O\left(e^{\frac{q\left(V_A + I_A \frac{N_S}{N_P} R_S\right)}{\eta_I N_S V_T}} - 1\right) - \frac{V_A + I_A \frac{N_S}{N_P} R_S}{\frac{N_S}{N_P} R_{sh}} \tag{8.8}$$

The basic open-circuit and short-circuit currents of a PV cell can be derived referring to Eq. (8.4) as given by respectively;

$$0 = I_{PV} - I_O\left(e^{\frac{V_{OC}}{\eta_I N_S V_T}} - 1\right) - \frac{V_{OC}}{R_{sh}} \tag{8.9}$$

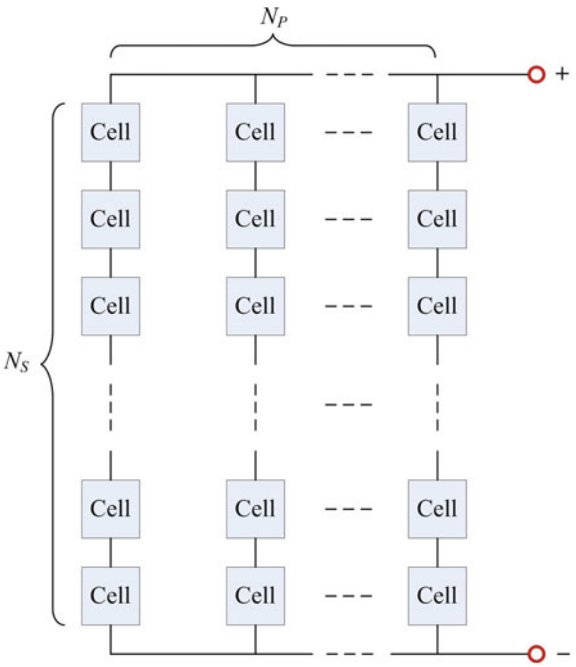

Fig. 8.3 Electrical connection diagram of a PV array

$$I_{SC} = I_{PV} - I_O\left(e^{\frac{I_{SC}R_S}{\eta_I N_S V_T}} - 1\right) - \frac{I_{SC}R_S}{R_{sh}} \tag{8.10}$$

The verification of a PV model is performed by measuring the current-voltage *I-V* and power-voltage *P-V* curves against various irradiation values. It is clear that the basic maximum power current–voltage pair belongs to the *I–V* characteristic that Eq. (8.4) is recalled to define the following maximum power relation;

$$I_M = I_{PV} - I_O\left(e^{\frac{V_M + I_M R_S}{\eta_I N_S V_T}} - 1\right) - \frac{V_M + I_M R_S}{R_{sh}} \tag{8.11}$$

A PV module is modeled referring to the relations given above that define the effect of R_s, R_{sh}, I_o, I_{PV}, and η. The curves shown in Fig. 8.4 are produced by changing the irradiation value from 200 W/m^2 to 1000 W/m^2. The axis on the left-hand side of figure represents the current variation I-V curve, while the right-hand side illustrates the output power of PV panel in terms of P-V curve. The effect of irradiation on current, power, and voltage can be easily seen from the graphic. The curves generated by the modelled PV panel are verified by comparing to datasheet of commercial PV modules at 240 Wp power [13].

The parameters of the modeled PV module are given in Table 8.1 where each parameter is verified in the simulation studies. The values are provided for 25 °C cell temperature and 1000 W/m^2 irradiation level.

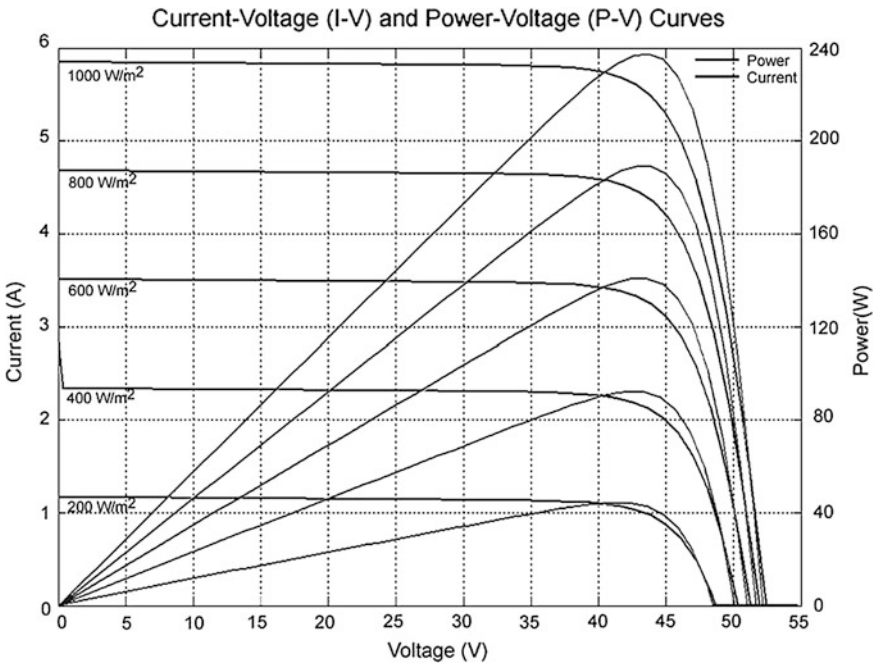

Fig. 8.4 I-V and P-V characteristics of a 240 Wp PV module at various irradiation conditions

Table 8.1 Electrical parameters of the modeled PV module [13]

Quantity	Value
Rated power (Pmax)	240 W
Open circuit voltage (V_{OC})	52.4 V
Maximum power voltage (V_{MPP})	43.7 V
Short circuit current (I_{SC})	5.85 A
Maximum power current (I_{MPP})	5.51 A
Temperature coefficient (P_{Max})	–0.30%/°C
Temperature coefficient (V_{OC})	–0.126 V/°C
Temperature coefficient (V_{SC})	1.76 mA/°C
Module efficiency	19%
Nominal operating cell temperature	48.3 °C

8.3 Power Conversion and MPPT

The solar power generation systems have attracted extensive attention in several application areas such as agricultural, residential, and even industrial sites. Furthermore, the sensations related to greenhouse emissions and carbon footprints are key factors to promote the utilization of solar power systems. Nowadays, the installation costs are decreased and overall efficiency of a PV system is increased

comparing to a few decades ago. The decreased costs allow redeeming earlier by ranging five years to seven years that accelerate the usage of solar energy in distribution systems. The solar power generation systems are constructed in two types; either standalone or grid-tied [14–17].

The standalone systems are attractive for remote sites where the distribution lines are unavailable. The standalone plants are composed of solar arrays, dc-dc converter, ESS, and inverter. On the other hand, the grid-tied systems eliminates ESS requirement and requires a grid-tie inverter instead of classical inverters. The complete block diagram of a solar power generation system with grid-connection is depicted in Fig. 8.5. The solar array is a combination of PV modules in series and parallel to generate the required power in various voltage and current ratings. The power conversion stage consists of dc power interface and its ac conversion pairs. The dc-dc converters are used to stabilize the intermittent characteristic of solar array that is considerably depended to solar irradiation and ambient temperature. The power conversion structure can be in single-stage or double-stage interface where the single-stage includes just a dc-ac inverter while the double-stage is composed of dc-dc converter and dc-ac inverter as seen in Fig. 8.5. The single-stage interface lacks in the stabilizing the dc bus voltage against rapidly varying dc output of solar array. However, the inverter requires operating an algorithm to track the maximum power point in order to match dc bus voltage of solar array.

However, it is not possible to sustain optimum matching at all radiation levels since the maximum power point rapidly fluctuates depending to the radiation and temperature. This operation can be performed in large-scale solar plants where the generated dc bus voltage excesses the required supply voltage of inverter. Therefore, the most proper way is to use double-stage power interface in any case [4, 16, 18–20].

A dc-dc converter is connected between solar array and inverter to match the required dc bus voltage in the double-stage power conversion system. The dc-dc converter handles the MPPT operation and the dc bus voltage is matched at this first stage. The MPPT algorithm of converter increases or decreases the dc bus voltage

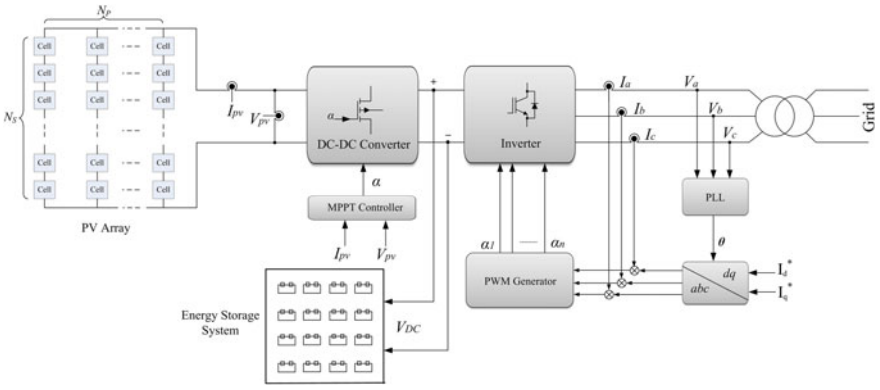

Fig. 8.5 The detailed block diagram of a solar power generation system

according to varied climatic conditions and maintains the match between dc supply limits of inverter. The MPPT algorithm controls the duty cycle of dc-dc converter where it changes the converted dc voltage level by adjusting the operation period of semiconductor switch in the topology. Thus, the maximum power is extracted from solar array by appropriately matching I-V balance of solar modules. The widely used dc-dc converter topologies are Buck-Boost and Cuk besides classical buck or boost topologies in solar power generation systems. It is not placed in this section since the converter topologies can be found in several textbooks [4, 20, 21].

The second interface used in double-stage is inverter that converts the dc bus voltage to ac power where the converted ac power is either supplied to the standalone loads or is injected to the utility grid. The inverter topology to be used in this interface depends to the power level where two-level or multilevel topologies can be selected. The multilevel topologies that were firstly introduced by Nabae generate the third voltage level with the neutral point of dc bus. The most widely used multilevel inverter (MLI) topologies are diode clamped, flying capacitor, and cascaded H-bridge in renewable energy. The diode clamped and cascaded H-bridge topologies provide the most proper involvement in high power applications where megavolt-ampere MVA power handling is desired. The flying capacitor arrangement eliminates filtering requirement comparing to diode clamped topology. However, this circuit is not accepted as robust as cascaded H-bridge to obviate the harmonic contents and the cost issues. Furthermore, several other MLI topologies such as grid-tied or string structures are implemented depending to the power ratings in solar energy application [4, 20].

The efficiency of a power conversion system is related to several factors such as conduction losses, switching losses, electromagnetic interference (EMI), and total harmonic distortion (THD) rates. The power efficiency is primarily decreased by power loss that are caused by active devices while the EMI and THD losses induce to defects on power quality and efficiency. The power losses increase proportionally to the switched voltage and current rates. The MLI topologies decrease the switched voltage and current rates at each cycle owing to its staircase output waveforms. Consequently, the power losses are also decreased comparing to regular two-level inverter topologies. The harmonic contents, THD ratios, and EMI rates are reduced by this way. The MLI output waveforms, either voltage or current depending to the topology, are increased to several levels, are particularly presented in odd numbers such as 3-level, 5-level, 7-level etc. In addition to these, the asymmetrical MLI topologies allow generating more increased output voltage levels by using same power stages as cascaded topologies [4, 19–21].

The rated power of a solar power generation system is increased by several string connections of power modules where the series-connected PV modules comprise the strings. Furthermore, several strings can be connected in parallel to achieve higher power ranges. The grid connection of PV plants that are constructed by using such strings is performed with various converter infrastructures. The most widely used power conversion schemes are illustrated in Fig. 8.6 where the connection diagrams of central converter, multi-string converter, string converter, and micro-converter are exhibited from Fig. 8.6a–d, respectively. Central converters are

constituted of inverters that convert the dc voltage achieved from PV strings ac voltage. They are widely used in residential, commercial, and utility scale systems with a power level of 1 kW or higher. The MPPT operation of the PV panels is performed centrally at the dc-ac inverter stage as shown in Fig. 8.6a. The main advantages of this scheme are decreased cost of inverter and decreased switching losses owing to unique converter structure. However, the central converter usage causes to a main drawback in acquired energy level since it is controlled by a single MPPT where the individual MPPT support is not available for each PV strings. Thus, the acquired maximum power level is limited under shading, thermal variations, aging or disorientation of PV strings. The multi-string converter seen in Fig. 8.6b is comprised of several individual dc-dc converters usually managing two

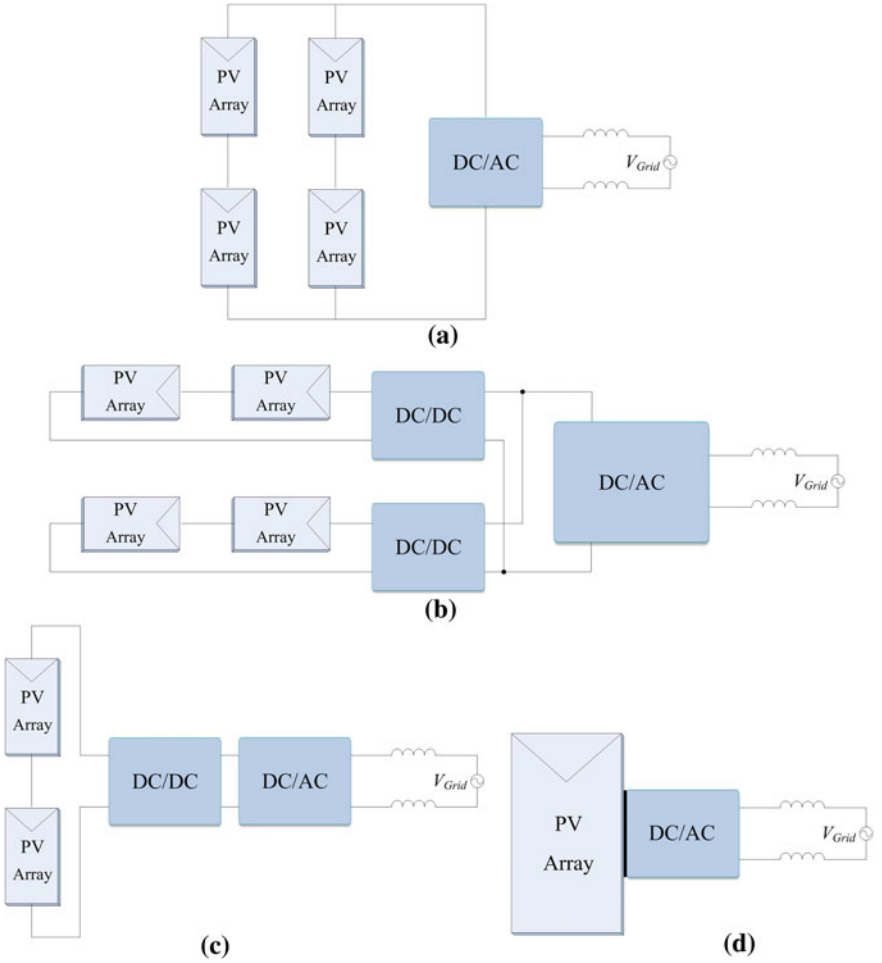

Fig. 8.6 Power conversion schemes in grid-tied PV systems, **a** central converter, **b** multi-string converter, **c** string converter, **d** micro-converter

PV strings or three PV strings at most. In this case, the double-stage interface is compulsory. The most important contribution of the double-stage interface is additional dc-dc converters that allow increasing the dc input voltage in a wide range. The PV plant can be freely constructed by arranging several dc-dc converter connections of strings. The dc-ac conversion is configured by using a central inverter that eliminates the drawbacks of the previous converter structure since the MPPT operations are handled by dc-dc converters.

The string converter that is shown in Fig. 8.6c is configured with individual MPPT controllers that do not allow parallel connection of strings. This option provides to locate each PV string in any direction or orientation. Furthermore, it is freely possible to care shading conditions and to determine PV module number in a string. The prominent feature of string converter is relevant to its power level that is widely designed at low power levels to be used in single-phase applications. In addition to this, its common topology includes full-bridge inverter with lien frequency transformer at the output stage. Thus, this configuration causes to a drawback of higher cost per kW. The micro-inverter is constituted with a dc-ac converter for each PV module where individual MPPT and power conversion features are acquired by this way. The configuration seen in Fig. 8.6d enables each PV module to connect to the ac grid without any dc wiring. Although this configuration provides simpler usage and installation, the cost per kW is higher than string converters.

Also, the operation cycle of the converter is lower than of a PV module [20, 21]. Although the utilization of PV systems are increased day by day, two main drawbacks are being extensively studied to overcome which are high installation costs, and low conversion efficiency. The acquired output power of a PV system is increased by using several mathematical algorithms. The MPPT is a fundamental method that eliminates the mismatch along the load characteristic and maximum power output of a PV module. MPPT algorithms ensure the optimal usage of PV modules against several defective conditions such as disorientation, shading or partial shading. Furthermore, the intermittent characteristic of solar power is sustained in a reliable way by using MPPT methods. Many MPPT methods have been proposed for single-stage and double-stage systems to cope with performance limitations. The most prominent classifications of MPPT methods are indirect and direct methods. The indirect methods include several algorithms such as open-circuit, constant voltage, short-circuit, and pulse method where some of them requires former knowledge on the PV array characteristics while some requires mathematical calculations. These requirements limit the efficiency of the algorithm at any case of irradiance and temperature variations.

The alternative MPPT methods are classified under direct methods where the most widely known ones are perturb and observe (P&O), hill climbing (HC), and incremental conductance (IncCon). These methods are competitor to indirect methods in terms of simplicity, easy implementation with limited prior information, and efficiency The commercial applications of MPPT methods are performed with P&O algorithm where the algorithm instantly measures voltage value at the maximum power point and tracks the variation. The MPPT algorithm is used to determine the switching angle of power converters depicted in Fig. 8.6. The algorithm detects and

tracks the reference voltage to change the duty cycle, and consequently the output voltage of converter [4, 22–25]. The most recent improvement of MPPT algorithms are performed by using intelligence based methods such as fuzzy logic controllers (FLCs), artificial neural networks (ANNs), particle swarm optimization (PSO) algorithms, and several genetic algorithm (GA)methods [23, 26]. The soft computing methods provide better efficiency and faster response comparing to indirect and direct methods. However, they lack on simplicity. The MPPT methods and outstanding properties are presented in the following sections.

8.4 Indirect MPPT Algorithms

The indirect MPPT algorithms differ from direct MPPT methods by calculations to determine the PV cell voltage and current at MPP. However, the direct MPPT methods are based on measurements instead of calculations. The indirect algorithms are based on several calculation methods including system voltage adjustment, temperature measurement, open-circuit voltage VOC calculation, and azimuth and angle calculation sometimes. The system voltage or operating voltage adjustment is performed to detect the MPP voltage according to seasonal variations where it should be higher in winters. The operating voltage depends on the PV module temperature. The MPP voltage is calculated regarding to VOC that is instantly measured. The main advantage of indirect MPPT methods including constant voltage, open-circuit voltage, and short-current pulse-based is their simplicity. However, they lack against aging and pollution of PV cells [26–29].

8.4.1 Constant Voltage MPPT Method

The constant voltage (CV) method is the plainest MPPT algorithm that is based on regulating the array voltage to track the MPP voltage V_{MPP} as seen in Table 8.1. The PV array voltage is adjusted around V_{MPP} regarding to the reference voltage V_{Ref} that is the regulated array voltage. It is intended to match the V_{Ref} to V_{MPP} in the most proper adjustment. If this is not the case, then the algorithm tries to acquire the most adequate adjustment around the V_{MPP}. The CV algorithm assumes that the irradiance and temperature variations on the cells do not cause to meaningful changes on V_{MPP} and therefore, the V_{Ref} can be kept constant during the operation of algorithm. The flowchart of the CV MPPT operation is illustrated in Fig. 8.7 where the PV array voltage is required to be measured at the beginning of the algorithm. The algorithm does not involve any other input data. The measured array voltage V_{PV} is used to set up the duty-cycle of dc-dc converter. Then the duty cycle is updated at each turn by comparing the array voltage to reference voltage [26, 28]. When the array voltage is greater than reference, the duty cycle is decreased in the next step or vice versa.

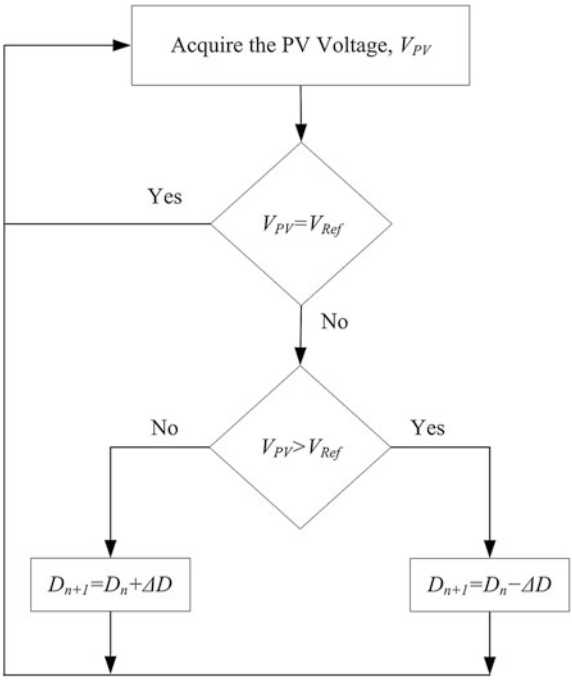

Fig. 8.7 Flowchart of the constant voltage MPPT method

It should be noted that CV method is more efficient comparing to regular P&O technique during the lower irradiance conditions. Therefore, it may be integrated other MPPT methods.

8.4.2 Open Voltage MPPT Method

The open voltage (OV) method is based on the assumption of that V_{MPP} is ever around a fixed percentage of the open-circuit voltage V_{OV}. It is also assumed that the production variations of cells, temperature, and solar irradiance rates change the MPP around 2% of its regular value. Therefore, this method defines a reference voltage V_{Ref} at the 76% of V_{OV}, which is quite near to V_{MPP}.

The flowchart of OV method is depicted in Fig. 8.8 where open-circuit voltage V_{OV} measurement is required to determine the reference voltage. This measurement is performed by opening the circuit, and a series static switch is used to carry out this action. This operation causes to zero PV current that prevents the power generation at this stage. In the next step, the measured PV voltage V_{PV} is compared to the reference voltage V_{Ref} to determine the exact duty-cycle of dc-dc converter. The pre-defined duty-cycle D_n is increased in the next step, if V_{Ref} is greater than V_{PV} [26, 28, 30, 31].

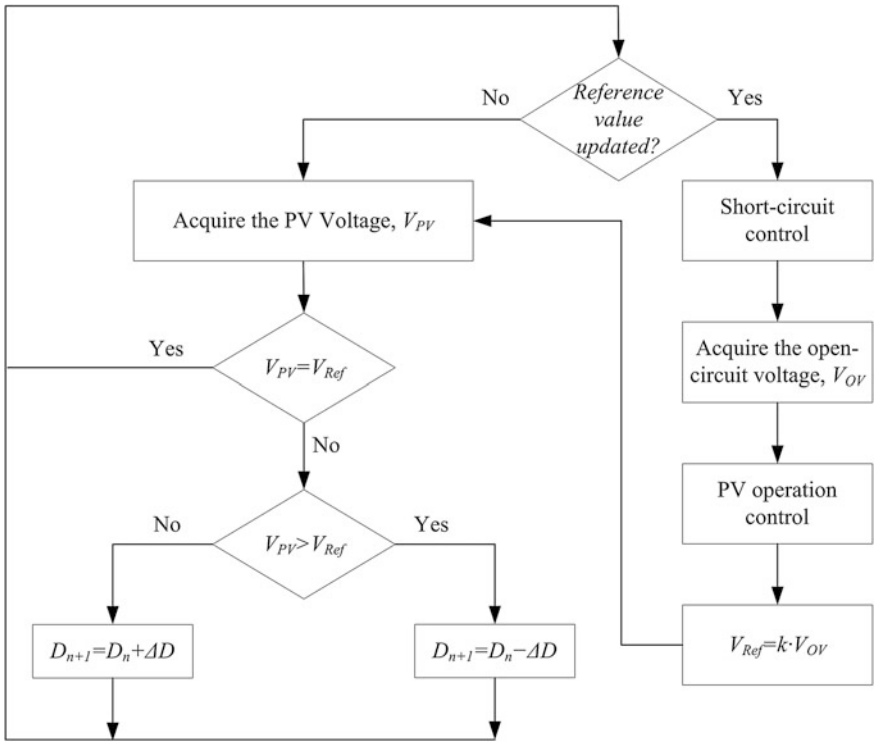

Fig. 8.8 Flowchart of the open-voltage MPPT method

If the V_{PV} is greater than V_{Ref} then the D_n is decreased by varied value for the next duty-cycle calculation D_{n+1}. The regulated dc output voltage is controlled by PI block at each cycle to track the V_{MPP}.

8.4.3 Short-Current Pulse-Based MPPT Method

The short-current pulse-based (SCPB) MPPT method determines V_{Ref} that is required to generate the optimum operating current I_{OP}. In the ideal conditions, I_{OP} is proportional to the short-circuit current I_{SC} by a coefficient k and irradiance level of S as seen in Eq. (8.12);

$$I_{OP}(S) = k \cdot I_{SC}(S) \tag{8.12}$$

The equation exhibits that the operating current is defined by irradiance level and ISC where it is also temperature dependent that varies between 0 and 60 °C. On the other hand, the coefficient is assumed to be around 92%. It is obvious that this

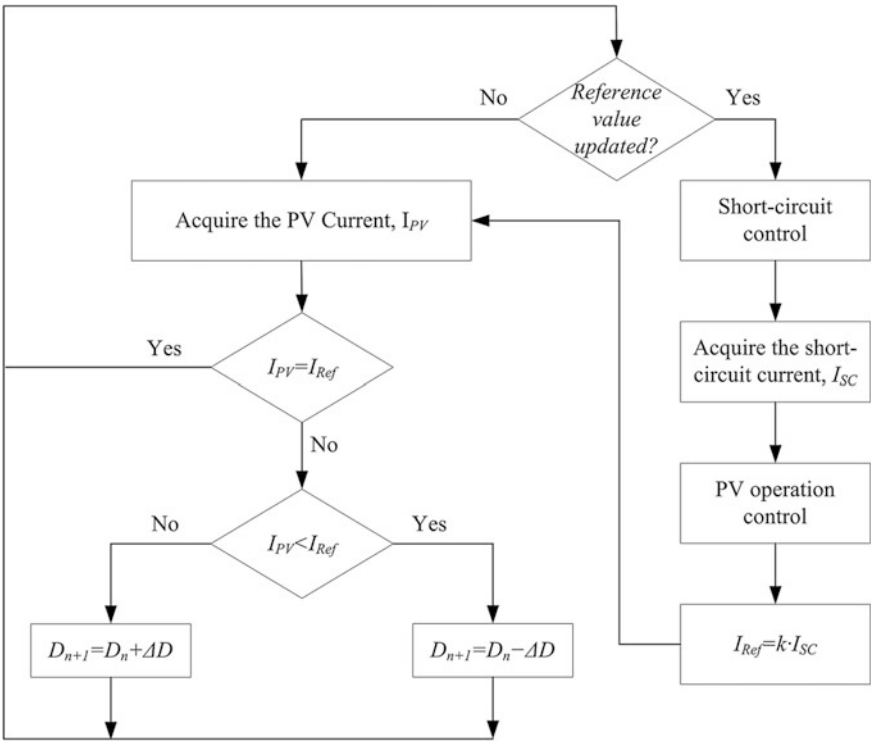

Fig. 8.9 Flowchart of the short-current pulse-based MPPT method

algorithm is based on short-circuit current measurement and that is performed by a parallel static switch similar to previous method. The parallel switch provides the short circuit conditions where the array voltage is zero and power generation is prevented. The flowchart of this control method is shown in Fig. 8.9 that the preliminary measurements and comparisons are depicted similar to OV MPPT algorithm with a difference where the measured and compared parameters are current in this method [27, 28, 30, 31].

The PI regulator requires the array voltage as in the OV method to generate the operating current where the reference voltage is also acquired at this stage.

8.5 Direct MPPT Algorithms

The direct MPPT algorithms are based on measurement of PV module voltage, current, or instant power where the performance variations are rapidly detected and more accurate tracking is performed. The basic principles of direct MPPT

algorithms are related to periodic tuning of I-V and P-V curves, and adjusting the operating voltage in small steps to increase the accuracy. The first principle is used to determine the maximum output power of PV module that is tracked at each turn of duty-cycle calculation of the dc-dc converter. The second principle is performed by a method known as hill climbing that is based on detecting the power or current direction either increasing or decreasing. In case the measured value increased depending on the operating voltage, the tracking direction is set to forward, otherwise it is set to backward. The MPP is detected by this principle and the operating point track the real MPP with little oscillations regarding to step size [24, 25, 29, 32]. The characteristics of a typical PV cell under regular irradiance and partial shading conditions are illustrated in Fig. 8.10 where the MPP dot depicts the current source and voltage source operation of PV module. If the operating point of the load is on the left-hand side of MPP, it means the module operates as a current source and the error signal M required by Hill-Climbing HC MPPT is calculated as given in (8.14);

If the operating point of the load is on the right-hand side of MPP, then PV module acts as a voltage source, and M is calculated as follows;

$$\frac{\partial P_{PV}}{\partial V_{PV}} > 0 \Rightarrow M = M + \Delta M \tag{8.13}$$

$$\frac{\partial P_{PV}}{\partial V_{PV}} < 0 \Rightarrow M = M - \Delta M \tag{8.14}$$

Apparently, the error signal will be zero at the MPP that yield $\Delta M = 0$. This approach is applied at several direct MPPT methods where the most outstanding algorithms are P&O and Incremental Conductance (IncCon) [29, 31, 32].

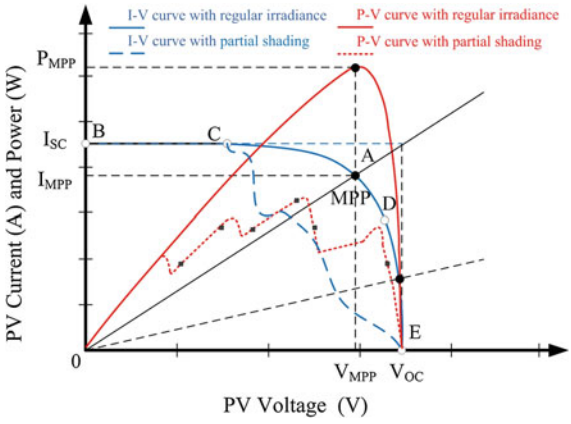

Fig. 8.10 Characteristics of a typical PV cell under regular irradiance and partial shading

8.5.1 Perturb and Observe MPPT Algorithm

The P&O algorithm is one of the most widely used and studied method owing to its simplicity and practical implementation. It perturbs the terminal voltage, as its name implies, and compares the actual PV power to previous value. The algorithm decides to track the MPP in one direction or in the opposite direction by comparing the terminal voltage change and output power increment. In case the output power is increased against the voltage change, the algorithm keeps on tracking the MPP in the same direction. Otherwise, it shifts the tracking direction [4, 26, 32, 33].

There are several textbooks and papers can be found on regular P&O algorithm in the literature. However, the main attention should be directed to improve instead of applying the regular P&O. The flowchart of an improved algorithm proposed by Dolara et al. [26] is shown in Fig. 8.11 where the power and voltage perturbations are detected in the progress, and then the voltage difference is detected to operate the algorithm. In the proposed method, the array power is sampled to generate an

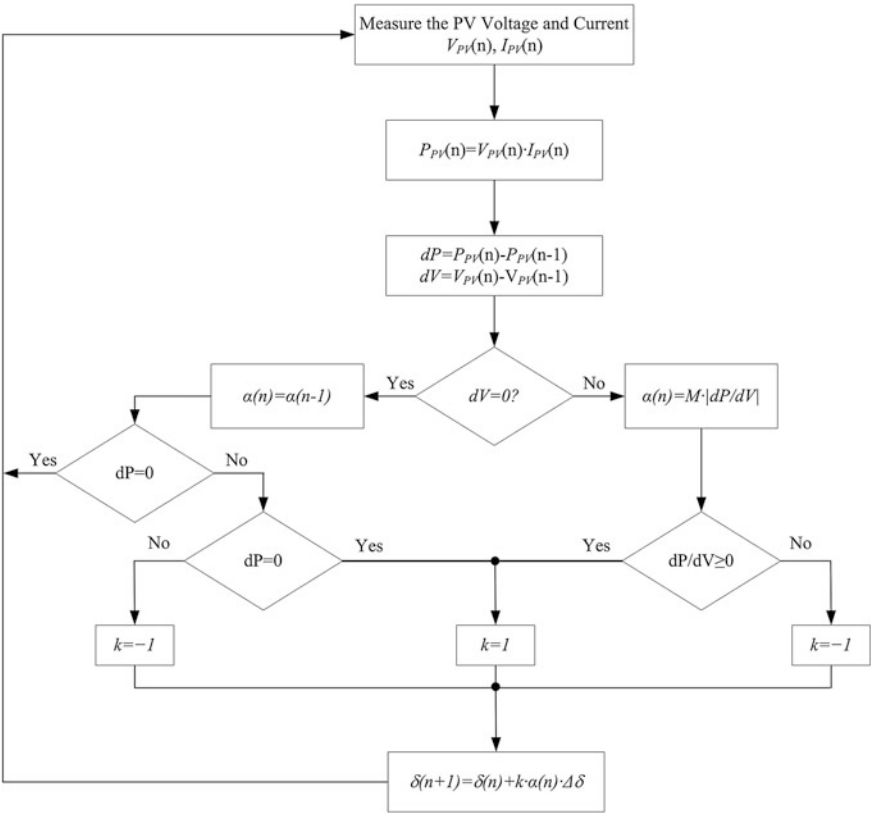

Fig. 8.11 Flowchart of optimized P&O MPPT method [26]

average value, and is used for arranging the magnitude of perturbation $\Delta\delta$ at the MPP operating point.

The arrangement is performed by calculating the $\alpha(n)$ regarding to voltage error signal M and power to voltage ratios as shown on the right-hand side of flowchart. The duty cycle is varied around 0.5% for each regular P&O methods. However, the proposed algorithm in [26] tries to adjust the duty cycle variation between 0.5% and 2.7% in the next turn regarding to k coefficient, α (n), and $\Delta\delta$ where it is equated as follows;

$$\delta(n+1) = \delta(n) \; + \; \mathrm{k} \cdot \alpha(n) \cdot \Delta\delta \tag{8.15}$$

An improved P&O MPPT method with PI control is proposed by Kabalci et al. [34, 35] where the schematic diagram of combined controller is illustrated in Fig. 8.12. The MPPT control of converters are improved with additional PI to regular P&O algorithm where measurements of solar array, dc converter, and control diagram of PI controller are shown on the left-hand side of Fig. 8.12. The flowchart of the improved PI controlled MPPT algorithm is depicted in Fig. 8.13 where additional PI calculation is managed by the error calculation segment on the flowchart.

The flowchart of MPPT algorithm is depended on voltage and power calculations that are based on current and voltage values acquired from sensors [34].

Once the actual power is calculated, then the next cycle of the measurement is compared to previous value to track the reference voltage V_{ref}. The implemented control section that the upper and lower parts of detailed PI controller block exhibit P&O detection part while the middle part on the left hand side of figure illustrates the PI control added to MPPT algorithm considering K_p and K_i parameters of the

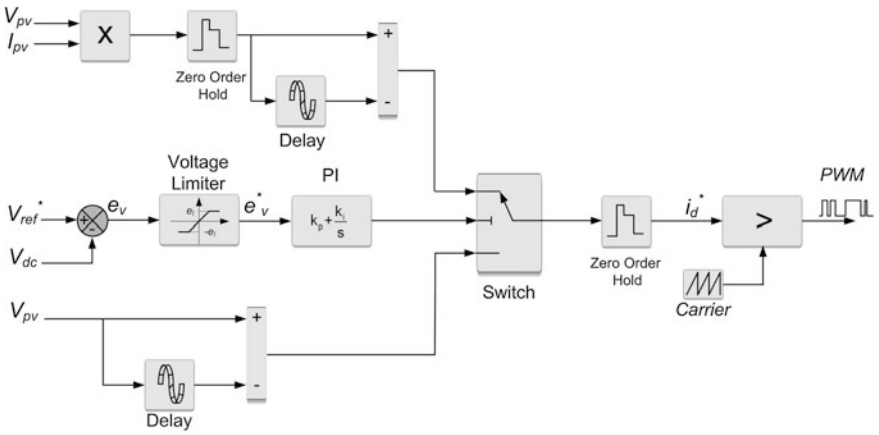

Fig. 8.12 Schematic diagram of the PI assisted MPPT [34]

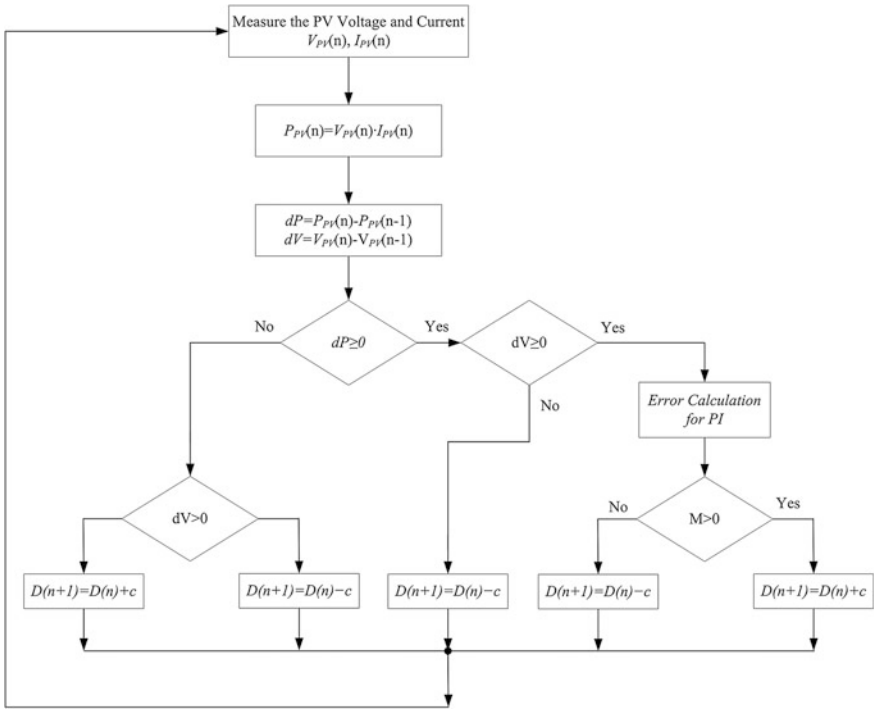

Fig. 8.13 Flowchart of optimized PI assisted P&O MPPT method [34]

system. The actual inputs and reference outputs are switched as seen in the center of PI controller block and modulating signal is conditioned by the zero-order sample and hold block. The logical comparator compares the triangular carrier signal and modulating signals to generate the PWM at each interval where the actual power measurement is repeated [34].

In order to determine duty ratio the latest observation of the obtained power is compared to the previous observation. Afterwards, ensured difference is used to specify the next PWM duty cycle. The implemented P&O algorithm looks for the increment of power perturbation and attempts to keep the duty cycle in the same way in order to achieve the MPP of PV array, also PI control is activated to reduce oscillation on the output voltage. The algorithm can reverse the perturbation when there is a decrement occurs in the power observation. The algorithm repeats this process for reach to MPP of PV array, if the system reaches to the MPP; the algorithm produces steady duty cycle value. The oscillation at the MPP of PV array is demanded to be reduced in order to increase the stability [35, 36]. The PI function, which is used to reduce oscillation on the output voltage is calculated as given in short code of Eq. (8.16) [35];

$$\left.\begin{array}{l} Void\_PI() \\ \{ \\ Error = Vref - Vo; \\ Error\_in = Error\_in + Error * dt; \\ duty = Error * Kp + Error\_in * Ki; \\ \} \end{array}\right\} \tag{8.16}$$

8.5.2 Incremental Conductance MPPT Algorithm

The incremental conductance *InCon* algorithm depends on the detection of the slope occurred in the PV curve. The slope is zero when the MPP of the curve is reached as shown in Fig. 8.10. The movement direction of operating point is detected by tracking the change occurred in the *I/V* ratio comparing to the MPP point. The operating point increases the slope when it is moving towards to the MPP, while it turns negative on the right side of MPP. This situation can be expressed as follows [25, 37–39];

$$\begin{array}{l} \dfrac{dI}{dV} = -\dfrac{I}{V}; \left(\dfrac{dP}{dV} = 0\right); \text{at MPP} \\ \dfrac{dI}{dV} > -\dfrac{I}{V}; \left(\dfrac{dP}{dV} > 0\right); \text{at left of MPP} \\ \dfrac{dI}{dV} < -\dfrac{I}{V}; \left(\dfrac{dP}{dV} < 0\right); \text{at right of MPP} \end{array} \tag{8.17}$$

The Eq. (8.17) and flowchart given in Fig. 8.14 are based on the instant conductance (*I/V*) and the incremental conductance (*dI/dV*) of PV array where the reference voltage is calculated regarding to incremental value in an iteration that is repeated until MPP is reached. Once the V_{Ref} acquired at the MPP, the algorithm maintains to track this value in order to ensure maximum output power. In case a change occurs in PV current *dI*, algorithm starts a new iteration at the beginning of the flowchart to track V_{Ref} by increasing or decreasing the previous value.

When the irradiance increases on the PV array, the array voltage is increased and the MPP moves to the right-hand side as can be seen on Fig. 8.10. The algorithm increases the operating voltage of PV array for compensating this increment. On the other hand, the decrement on irradiance triggers the algorithm to decrease the operating voltage of array in order to compensate the change. That is the way that InCon algorithm track the slope value to detect the change on irradiance and react against the cases. The easier way to determine the change is comparing previous and actual values of voltage and current that are depicted as *dV* and *dI* in the

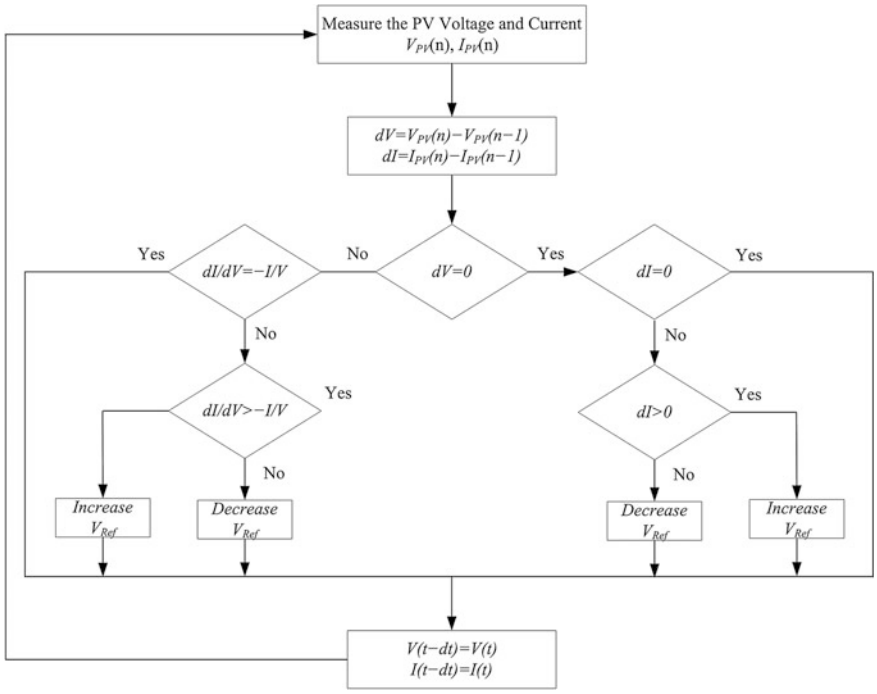

Fig. 8.14 Flowchart of incremental conductance MPPT method

algorithm. The *dV* and *dI* are zero when the irradiance and temperature are stable, and algorithm maintains to operate at MPP.

If the irradiance increases, it causes an increment on *dI* ($dI > 0$) while $dV = 0$ that also means the MPP is being increased by irradiance. The algorithm decides to increase the operating voltage at this stage. On the other hand, the decrement on irradiance causes to $dI < 0$ that requires to decrease the operating voltage. The rapidly changing cases are easily detected by InCon algorithm since it depends on tracking the operating point towards MPP. This approach prevents misleading in tracking as seen in P&O algorithm, and that makes InCon more reliable by decreasing the perturbation around MPP. However, there are several drawbacks of this algorithm related to MPP as others. Tey and Mekhilef [40] proposed an optimized alternative to regular incremental conductance method by increasing the step size that is named as variable step size InCon. The algorithm is based on defining a step size to compensate the variations on MPP change and increasing or decreasing the duty cycle considering this step size additional to previous duty cycle. Thus, an error rate is permitted by algorithm and the step size is adjusted to maintain the error control in the limit. There are several methods are proposed to optimize regular MPPT methods. However, the numerical methods including FLCs, Neural network controlled

algorithms, and some other soft computing methods are applied to improve existing methods. The rapidly adapting structures, complexity, and sophisticated approaches of these algorithms increase the reliability of regular MPPT methods.

8.6 Artificial MPPT Algorithms

The most widely used MPPT methods are introduced in 4th and 5th sections. There are several other methods are also proposed in the literature including non-linear and sliding mode control methods in order to improve the stability and efficiency of regular MPPT algorithms such as perturb and observer or incremental conductance. However, the main drawbacks seen in the proposed methods are caused by irradiation and cell temperature that are not robustly handled by existing algorithms. The widely known methods are based on discontinuous control strategy where the intersection tracking is performed around the MPP. The tracking approach of the previously introduced algorithms lack in efficiency since they are not supported by intelligent controls and are less efficient against the rapidly changing conditions [41–44]. Furthermore, the existing methods do not pay attention to measurement noises of voltage and current that has significant effect on the algorithm decisions.

These drawbacks require fast time response and increased stability comparing to widely known methods. The oscillations occurred in the acquired power output should be decreased in order to decrease power losses. The latest improvements in MPPT methods are performed by using several numerical and artificial methods including FLC, neural network, neuro-fuzzy, genetic algorithm, and some optimization algorithms such as particle swarm optimization, artificial bee colony etc. The FLC is one of the simplest algorithms among other artificial methods. Recently, an increasing attention paid to FLC based MPPT algorithms owing to its robust response against unpredictable air conditions and its simple structure not requiring complex mathematical arrangements. The neural networks are also being extensively studied owing to their high level control structure and sophisticated management features [42, 43]. The following subsections are dedicated to artificial methods used in MPPT algorithms with analyses.

8.6.1 Fuzzy Logic Control MPPT

The combining artificial intelligence with regular MPPT algorithms is a new trend of research and application in renewable energy sources. FLC is the most widely researched artificial method in MPPT applications since it provides better performance comparing the conventional methods, and involves simpler requirements comparing to sophisticate neural or estimation algorithms. These advantages of FLC are integrated to overall system by combining it to existing MPPT controller that provides to acquire maximum power transfer to the loads.

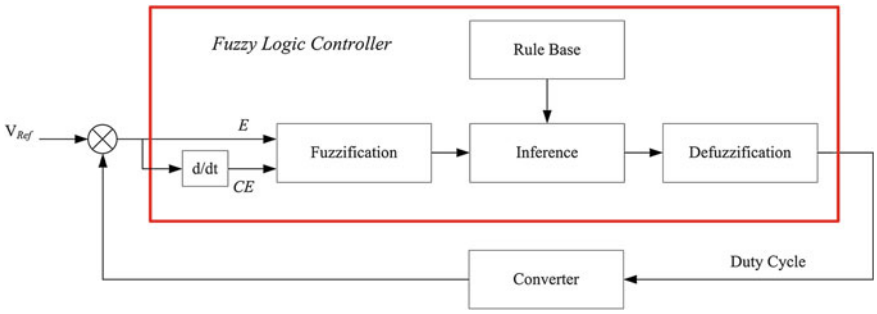

Fig. 8.15 Block diagram of a FLC MPPT controller

The block diagram of a FLC based MPPT controller is depicted in Fig. 8.15 where the contents of a regular FLC are also shown in a significant block. The reference input of FLC is used to determine the error signal *E* and change rate of the error *CE* where it is shown on the left-hand side of figure. The output of FLC is the duty cycle that is applied to converter where it is generated by the four sections of FLC. These sections are fuzzification where the numerical inputs are converted to lexical variables that are defined by rule base and depended to membership functions. The levels of membership functions can be increased to present better resolution in the calculations. The analyzed inputs are weighted according to several methods, namely modus ponens, Takagi-Sugeno or Mamdani, in the inference section, and then the lexical outputs of FLC are converted to numbers in the defuzzification section in order to generate the duty cycle. The most widely used defuzzification method is the is the centroid of area (COA) owing to its successful averaging properties and more accurate results [41, 42, 44]. The integration of FLC to the regular P&O algorithm is illustrated in Fig. 8.16 where the decision making against output power is performed regarding to the power and voltage perturbation by FLC controller that generates the adaptive duty cycle.

8.6.2 Neural Network MPPT

The most recent researches on computational MPPT methods include ANN studies that are significantly effective on wide disruptive conditions such as partial shading [45, 46]. The ANN based MPPT provides rapid and reliable estimations against quickly varying irradiance and temperature parameters. An ANN is composed of several layers in multilayer perceptron (MLP) structure as shown in Fig. 8.17. In a model as shown in figure, the neural-like organization is comprised of neurons seen in the lower part of figure where the inputs are linearly weighted and summed in a function. The sum of weighted input are transferred to a nonlinear function called

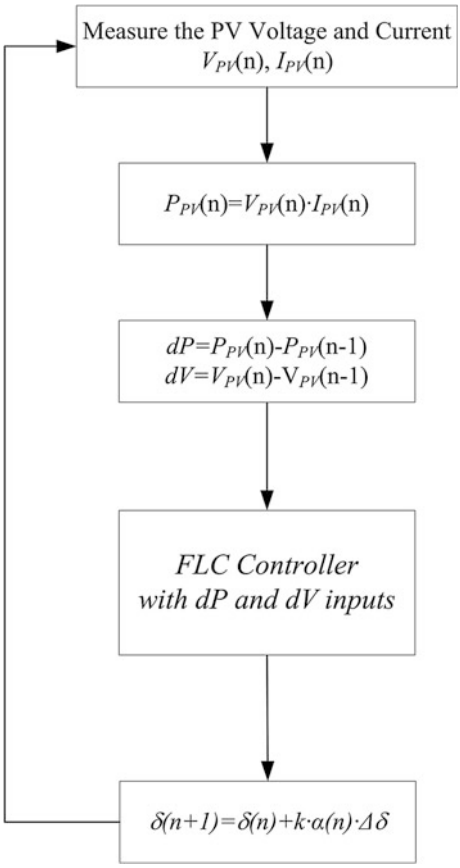

Fig. 8.16 Flowchart of a FLC P&O MPPT algorithm

activation function (AF), and lastly are sent to the following neurons. The definition of input function in AF is depicted as given in Eq. (8.18);

$$x = \sum_{m=1}^{M} w_m x_m + \alpha \tag{8.18}$$

where $x_1, x_2, \ldots, x_m$ are input signals, and $w_1, w_2, \ldots, w_m$ are the weights of each input signal [45].

The weights define the significance of each input data and the learning operation of the network is performed regarding to continuously varying weights. The training set of the ANN is composed with several different input and output data where they are voltage and current in inputs and MPP voltage at the output as seen in Fig. 8.17. There are several ANN based MPPT operation approaches are proposed. In one hand, some ANN algorithms integrated to regular MPPT methods use irradiance and temperature measurement acquired from separate sensors and

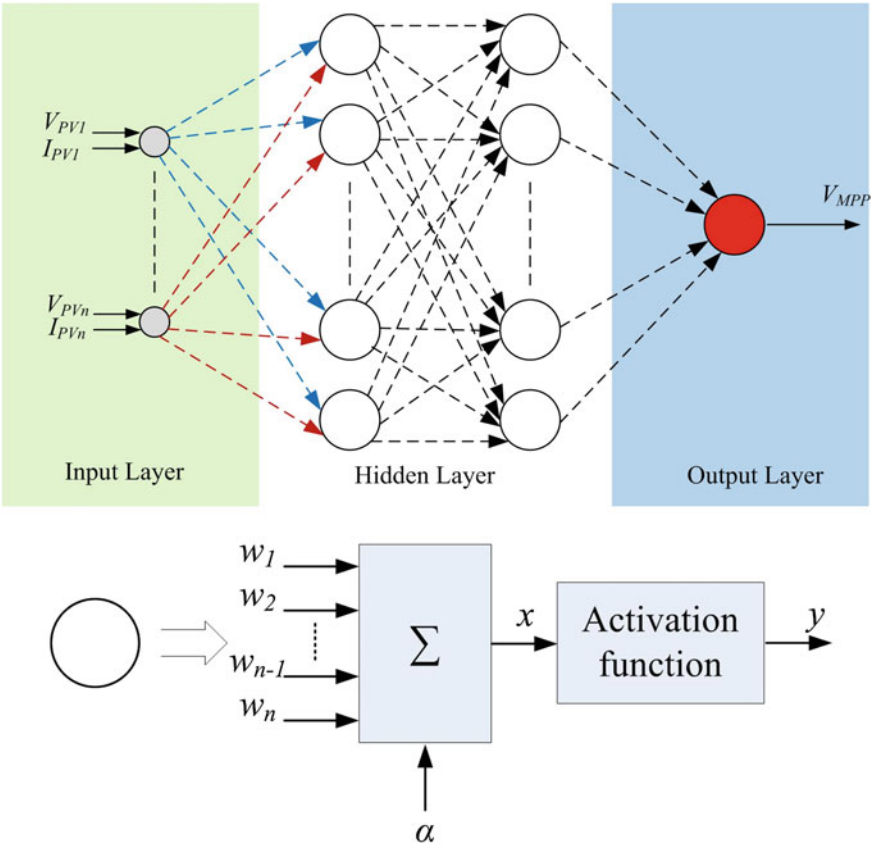

Fig. 8.17 Block diagram of an ANN controlled MPPT algorithm

directly generates variable duty cycle. On the other hand, the measured irradiation and temperature data are used to detect the voltage and current of PV module in other ANN MPPT group. The second group is widely used rather than first one and it is constructed with MLP structure [46–48].

8.6.3 Particle Swarm Optimization MPPT Algorithm

Particle swarm optimization *PSO* is a novel swarm optimization algorithm that is firstly proposed by Kennedy as an evolutionary algorithm based on behavior of birds [49, 50]. PSO uses a set of particles that each one suggests a solution to the optimization problem. It is based on the success of all particles that emulates a population where the position of each particle depends to the agent position to

detect the best solution P_{best} by using current particles in the population G. The position of any particle x_i is adjusted by

$$x_i^{k+1} = x_i^k + v_i \tag{8.19}$$

where the velocity component v_i represents the step size and is calculated by using the Eq. (8.20);

$$v_i^{k+1} = \omega v_i^k + c_1 r_1 (P_{best\_i} - x_i^k) + c_2 r_2 (G - x_i^k) \tag{8.20}$$

where ω is the inertial weight, c_1 and c_2 are the acceleration coefficients, r_1 and r_2 are random values that belong to the interval of [0, 1], P_{best_i} is the best position of particle i, and G is the best position in the entire population [50].

A typical MPPT method should be used to integrate PSO algorithm to controller. Most widely used integration is based on hill-climbing or P&O algorithm to PSO. The flowchart of a PSO MPPT algorithm is depicted in Fig. 8.18. The operation given in flowchart can be analyzed in five steps that are *initialization, fitness evaluation, updating the individual and global best value, updating the velocity and position of each particle,* and *convergence determination* [51]. In the first step, particles are randomly initialized in the distribution space, or are initialized on

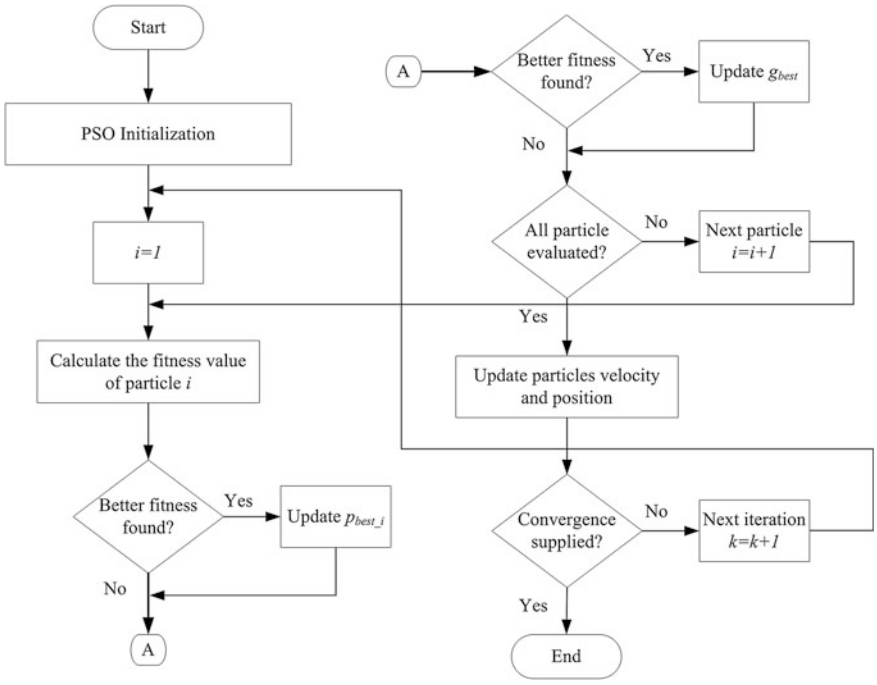

Fig. 8.18 Flowchart of PSO MPPT algorithm

described grid nodes covering the search space. Similarly, the initial velocity values are defined randomly. The fitness value of each particle is evaluated in the second step where the fitness evaluation is leaded to provide candidate solution to the objective function.

The individual and global best fitness values are determined in the third step where p_{best_i} and g_{best} are respectively determined. Then the positions are updated and replaced with better fitness values if they are found. The velocity and position of each particle are updated in the fourth step respecting to Eqs. (8.19) and (8.20). The last step of the flowchart checks the convergence criterion. If the criterion is met, the process is finished. Otherwise, the iteration number is increased and procedure returns to step 2 [51–53].

The application of PSO MPPT in a PV system is depended to the matching definitions of both systems. The particle positions are used to define the duty cycle of dc converter, and the fitness value evaluation function stands for the output power of PV array. The success of algorithm is performed by increasing the number of particles that provides more accurate MPP tracking operation, even for shading problems. On the other hand, increased number of particles causes to longer computation times. The particle number is usually selected as the number of series connected cells in a PV array in order to obtain the most exact operation time.

The particles are placed either on fixed positions or on random places in the PSO initialization step. It depends on the information about global MPP since the particles can be placed around the point, if there is any information about it. The PV voltage and current are measured and digitally filtered by using finite impulse response filters in order to calculate the fitness value, P_{PV} of particle i. The calculated fitness value is compare to the best fitness value in order to keep p_{best_i} or to update it with the new p_{best_i} in case of better fitness value. The velocity and positions of all particles are updated and convergence criteria are controlled to generate the best control signal [51–53].

The dependency to $p_{\text{best\_i}}$ and g_{best} is the main problem of conventional PSO algorithm under nonlinear shading conditions. Since there are several PSO methods proposed in the literature. The outstanding alternative to classical PSO are deterministic and dormant PSOs [52, 53].

8.7 Conclusions

This chapter deals with most widely used and recent trends in MPPT algorithms. The literature reviews show that several methods are proposed to track the MPP in a PV power system. The main concerns of all the proposed algorithms are fast response, reliable tracking, and easy implementation. The power conversion devices and configurations are improved to increase acquired energy level of a solar plant. Although there are various structures proposed in literature, double-stage power conversion holds the great share of usage in residential and industrial plants. The first stage is comprised of dc-dc converters while the second stage performs

dc-ac conversion by using inverters. The dc interface requires robust control methods to increase converted energy under heavily or partially shaded conditions. The MPPT algorithms are focused on coping with irradiance and temperature variations to balance the acquired total output power.

The preliminary algorithms classified as indirect algorithms are based on several calculation methods including system voltage adjustment, temperature measurement, open-circuit voltage V_{OC} calculation, and azimuth and angle calculation sometimes. These methods lack on responding against rapidly changing weather conditions. The direct methods that includes hill-climbing, P&O, and indirect conductance are proposed to tackle this situation. The basic operation principles of direct MPPT algorithms are based on periodic tuning of *I-V* and *P-V* curves, and adjusting the operating voltage in small steps to increase the accuracy. The decreased step size and effective measurement methods increased the reliability of direct MPPT methods. However, the researches exhibited the perturbation issue seen around the MPP can be overcome with computational methods. Their simple analytical background led the main drawback of direct methods. Therefore, more sophisticated and complex algorithms were researched to prevent the perturbations occurred in power curve of PV arrays.

A wide variety of numerical methods including fuzzy logic, neural networks and other computational methods are proposed. The most recent computational algorithms including GAs, PSO algorithms, and ABC are prominent topics in MPPT algorithms. The trade-off between conventional MPPT methods and recent algorithms are related to complexity in algorithm and increased cost in application. However, improved efficiency and fast response leads to extensive researches.

References

1. Twidell J, Weir T (2006) Renewable energy sources. Taylor & Francis, London ISBN 0-419-25330-0
2. Kabalcı E, Kabalcı Y, Develi I (2012) Int J Electr Power Energy Syst 34:19–28
3. Masters GM (2004) Renewable and efficient electric power systems. Wiley-IEEE Press. ISBN: 13: 978-0471280606
4. Colak I, Kabalci E (2014) Chapter 7-Control methods applied in renewable energy, use, operation and maintenance of renewable energy systems. Springer, pp 205–246. doi:10.1007/978-3-319-03224-5_7. ISBN: 978-3-319-03224-5
5. Zeman M (2014) Chapter 9-Photovoltaic systems, Delft University of Technology
6. Hersch P, Zweibel K (1982) Basic photovoltaic principles and methods, SERI/SP-290-1448 solar information module 6213. Golden, Colorado
7. Gray JL (2003) In: Luque A, Hegedus S (eds) Handbook of photovoltaic science and engineering. Wiley, West Sussex, pp 61–112
8. Kabalcı E, Gokkus G, Gorgun A (2015) 7th international conference electronics, computers and artificial intelligence, Bucharest, Romania, 25–27 June 2015, pp SG23–SG28
9. Lineykin S, Averbukh M, Kuperman A (2014) IEEE Trans Ind Electron 61:6785–6793
10. Kadri R, Gaubert JP, Champenois G (2012) IEEE Trans Power Electron 27:1249–1258
11. d'Alessandro V, Guerriero P, Daliento S, Gargiulo M (2011) Solid State Electron 63:130–136
12. Tian H, David F, Ellis K, Muljadi E, Jenkins P (2012) Sol Energy 86:2695–2706

13. Panasonic HIT Photovoltaic Module, HIT Power 240S. http://www.panasonic.com/business/pesna/includes/pdf/eco-construction-solution/HIT_Power_SA06_Series_(240W)_Data_sheet-v2.pdf
14. Radjai T, Rahmani L, Mekhilef S, Gaubert JP (2014) Sol Energy 110:325–337
15. Pradhan R, Subudhi B (2015) Int J Electr Power Energy Syst 64:792–803
16. Mohanty P, Bhuvaneswari G, Balasubramanian R, Dhaliwal NK (2014) Renew Sustain Energy Rev 38:581–593
17. Bendib B, Krim F, Belmili H, Almi MF, Boulouma S (2014) Energy Procedia 50:383–392
18. Wu JC, Wu K, Jou HL, Chang SK (2014) IET Power Electron 7:2717–2725
19. Jiang J, Su YL, Shieh J, Kuo K, Lin T, Lin T, Fang W, Chou J, Wang J (2014) Appl Energy 124:309–324
20. Zheng H (2013) Solar photovoltaic energy generation and conversion—from devices to grid integration. PhD dissertation, Department of Electrical and Computer Engineering, Graduate School of The University of Alabama, Tuscaloosa, Alabama
21. Lorenzani E, Franceschini G, Bellini A, Tassoni C (2014) Chapter 6-Single-phase grid connected converters for photovoltaic plants, renewable energy. In: Hammons TJ (ed) InTech. ISBN: 978-953-7619-52-7
22. Rezk H, Eltamaly A (2015) Sol Energy 112:1–11
23. Bendib B, Belmili H, Krim F (2015) Renew Sustain Energy Rev 45:637–648
24. Sivakumar P, Kader AA, Kaliavaradhan Y, Arutchelvi M (2015) Renew Energy 81:543–550
25. Eltawil MA, Zhao Z (2013) Renew Sustain Energy Rev 25:793–813
26. Dolara A, Faranda R, Leva SJ (2009) Electromagn Anal Appl 3:152–162
27. Faranda R, Leva S; Maugeri V (2008) Power and energy society general meeting—conversion and delivery of electrical energy in the 21st century, 20–24 July 2008, pp 1–6
28. Faranda R, Leva S (2008) WSEAS Trans Power Syst 3:446–455
29. Onat N (2010) Recent developments in maximum power point tracking technologies for photovoltaic systems. Int J Photoenergy 1:1–11
30. Park M, Yu K (2004) In: 30th annual conference of IEEE industrial electronics society, pp 2040–2045
31. Coelho RF, Concer FM, Martins DC (2010) 2010 IEEE international conference on sustainable energy technologies (ICSET), pp 1–6
32. Rújula AA, Abián JA (2014) Sol Energy 109:95–104
33. Ahmed J, Salam Z (2015) Appl Energy 150:97–108
34. Kabalci E, Kabalci Y, Canbaz R, Gokkus G (2015) 4th international conference on renewable energy research and applications (ICRERA 2015), Palermo, Italy, 22–25 November 2015
35. Kabalci E, Gokkus G, Gorgun A (2015) ECAI 2015 7th international conference electronics, computers and artificial intelligence, Bucharest, Romania, 25–27 June 2015, pp SG23–SG28
36. Sea TY, Ka JS, Lee, CU, Chung DH (2013) 13th international conference on control, automation and systems (ICCAS 2013). IEEE
37. Hohm DP, Ropp ME (2003) Prog Photovolt Res Appl 11:47–62
38. Hsieh GC, Hsieh H, Tsai CY, Wang CH (2013) IEEE Trans Power Electron 28:2895–2911
39. Sera D, Mathe L, Kerekes T, Spataru SV, Teodorescu R (2013) IEEE J Photovoltaics 3:1070–1078
40. Tey KS, Mekhilef S (2014) Sol Energy 101:333–342
41. Mohd Zainuri MAA, Mohd Radzi MA, Soh AC, Rahim NA (2014) IET Renew Power Gener 8:183–194
42. Chiu C (2010) IEEE Trans Energy Convers 25:1123–1132
43. Chiu C, Ouyang Y (2011) IEEE Trans Control Syst Technol 19:1516–1526
44. El Khateb A, Abd Rahim N, Selvaraj J, Uddin MN (2014) IEEE Trans Ind Appl 50:2349–2358
45. Rizzo SA, Scelba G (2015) Appl Energy 145:124–132
46. Kofinas P, Dounis AI, Papadakis G, Assimakopoulos MN (2015) Energy Build 90:51–64
47. Khanaki R, Radzi MAM, Marhaban MH (2013) In: IEEE conference on clean energy and technology (CEAT 2013), pp 287–292

48. Messalti S, Harrag AG, Loukriz AE (2015) In: 6th international renewable energy congress (IREC 2015), pp 1–6
49. Shi J, Zhang W, Zhang Y, Xue F, Yang T (2015) Electr Power Syst Res 123:100–107
50. Mirhassani SM, Golroodbari SZM, Mekhilef S (2015) Int J Electr Power Energy Syst 64:761–770
51. Liu Y, Huang S, Huang J, Liang W (2012) IEEE Trans Energy Convers 27:1027–1035
52. Lian KL, Jhang JH, Tian IS (2014) IEEE J Photovoltaics 4:626–633
53. Ishaque K, Salam Z (2013) IEEE Trans Industr Electron 60:3195–3206